

GTP-21-1082

## The influence of cycle-to-cycle hydrocarbon emissions on cyclic NO:NO<sub>2</sub> ratio from a HSDI diesel engine

Felix Leach\*, Varun Shankar, Martin Davy

University of Oxford  
Oxford, UK

\* felix.leach@eng.ox.ac.uk

Mark Peckham

Cambustion  
Cambridge, UK

### ABSTRACT

Knowledge of the NO:NO<sub>2</sub> ratio emitted from a diesel engine is particularly important for ensuring the highest performance of SCR NO<sub>x</sub> aftertreatment systems. As real driving emissions from vehicles increase in importance, the need to understand the NO:NO<sub>2</sub> ratio emitted from a diesel engine during transient operation similarly increases.

Previous work by the authors identified significant differences in NO:NO<sub>2</sub> ratio throughout the exhaust period of a single engine cycle, with proportionally more NO<sub>2</sub> being emitted during the blowdown period compared to the rest of the exhaust stroke. At the time it was not known what caused this effect.

In this study, crank-angle resolved NO and NO<sub>2</sub> measurements using fast response CLD (for NO) and a new fast LIF instrument (for NO<sub>2</sub>) have been taken from a single cylinder high-speed light duty diesel engine at three different speed and load points including a point with and without EGR. In addition, crank-angle resolved unburned hydrocarbon (UHC) measurements have been taken simultaneously using a fast FID.

The NO<sub>x</sub> emitted per cycle and the peak cylinder pressure of that cycle have showed high correlation coefficients ( $R^2 < 0.97$  at all test points) in this work. In addition, a variation of the NO:NO<sub>2</sub> ratio through the engine's exhaust stroke is also observed indicative of in-cylinder stratification of NO and NO<sub>2</sub>. A new link between the NO:NO<sub>2</sub> ratio and the UHC emissions from an individual engine cycle is observed - the results show that where there are higher levels of UHC emissions in the first part of the exhaust stroke (blowdown), perhaps caused by injector dribble or release from crevices, the proportion of NO<sub>2</sub> emitted from that cycle is increased. This effect is observed and analysed across all test points and with and without EGR.

The performance of the new fast LIF analyser has also been evaluated, in comparison with the previous state-of-the-art and standard “slow” emissions measurement apparatus showing a reduction in the noise of the measurement by an order of magnitude.

## INTRODUCTION

Understanding and control of NO<sub>x</sub> emissions from diesel engines continues to be a significant topic of research interest [1]. On modern diesel engines these emissions are controlled using both in-cylinder techniques such as air/fuel mixture control [2], Exhaust Gas Recirculation (EGR) [3], as well as by aftertreatment devices such as Lean NO<sub>x</sub> Traps (LNT) and Selective Catalytic Reduction (SCR) catalysts [4, 5].

In this context, control of the NO:NO<sub>2</sub> ratio emitted from a diesel engine is of major importance as it has a material effect on the performance of engine aftertreatment technologies. For example SCR requires a 1:1 NO:NO<sub>2</sub> ratio for optimum efficiency [6]. A Diesel Oxidation Catalyst (DOC) is often used upstream of an SCR to promote this 1:1 ratio, however as fast warm-up catalyst technologies (such as close-coupled SCR where an SCR is upstream of a DOC [7]) become necessary for increasingly stringent Real Driving Emissions (RDE) legislation [1], engine-out control of this ratio increases in importance.

Given the thermal mechanisms which form NO and NO<sub>2</sub>, in general engine parameters which decrease total NO<sub>x</sub> emissions (NO + NO<sub>2</sub>) such as EGR lead to increases in NO<sub>2</sub>/NO<sub>x</sub> ratio (i.e. proportionally more NO<sub>2</sub>). This is because of the cooler temperatures preventing the conversion of NO<sub>2</sub> into NO [8].

Recent work has shown the effect of various engine parameters (such as humidity, inlet air temperature, EGR rate, fuel pressure, start of injection, and air-fuel ratio) on the NO:NO<sub>2</sub> ratio which can be used to control the ratio on an engine-out basis both at steady state [9] and in engine transients [10].

Previous work by the authors of this study [11] showed a close dependency on cycle NO<sub>x</sub> with the peak cylinder pressure of that cycle, but also revealed an unusual phenomenon which suggested that there was stratification of the NO and NO<sub>2</sub> in-cylinder at EVO. This showed, that on some engine cycles there was proportionally more NO<sub>2</sub> observed in the blowdown part of the exhaust stroke – implying that there was more NO<sub>2</sub> than NO near the exhaust valves. This led to what appeared as a slow rise rate of the NO signal when measured at crank-angle resolution. This effect occurred at all engine operating conditions, including a low temperature combustion (LTC) operating point, with and without EGR. An example of the comparatively slow NO rise rate is shown in Figure 1, which shows NO and NO<sub>x</sub> emissions from a series of seven complete combustion cycles at nominally constant engine load and speed. On three of these cycles (circled), there is clearly a slower rise rate of the NO emission, compared to the NO<sub>x</sub> emission which gives proportionally

more NO<sub>2</sub> in the blowdown part of the exhaust stroke. A detailed description of the analysis approach to a figure like this is given in the methodology section (see Figure 4 for example).

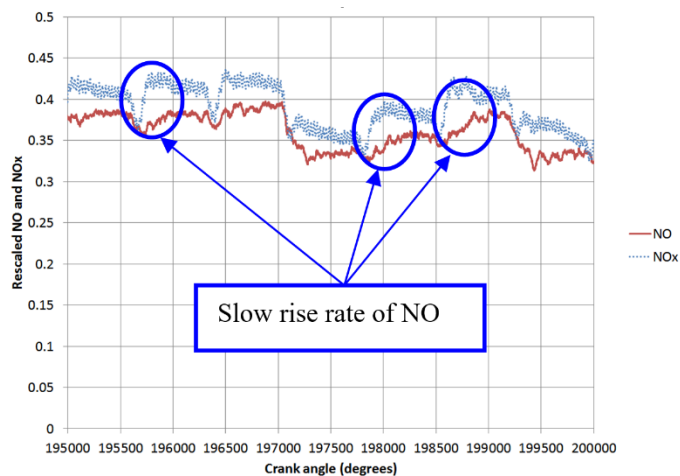
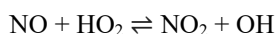


**Figure 1: NO and NO<sub>x</sub> emissions showing Slow NO rise rate in previous work [11].**

At the time of the previous study there was no clear indication as to the cause of the slow NO rise rate. The instrumentation was checked, and instrumentation effects and errors were ruled out. There was no fuel-bound nitrogen, which may have led to such a phenomenon. In addition, this slow rise rate of the NO did not occur on every cycle, it only occurred in approximately 50% of engine cycles (see Figure 1). Nothing was found in the literature which could explain it. The current work attempts to provide and test a hypothesis for the effect.

It is known that hydrocarbons (HC)s under certain conditions promote NO to NO<sub>2</sub> oxidation [12]. Hori *et al.* [13] conducted a series of experiments with a variety of different hydrocarbons and concluded that hydrocarbons that produce reactive radicals (particularly OH and monatomic O) are particularly responsible for this. Such radicals further consume the parent hydrocarbon and hence produce HO<sub>2</sub> radicals. These HO<sub>2</sub> radicals subsequently play a key role in NO → NO<sub>2</sub> conversion:



Subsequent work by Hori *et al.* [14] has shown that this reaction has a very strong temperature dependency (the highest relative levels of NO<sub>2</sub> – up to 100% - are seen in the range of 650 – 1000 K). A reverse reaction is also reported, at temperatures above 1000 K but this reaction requires a residence time of order 1 s.

These temperature conditions will occur during a typical combustion cycle in a diesel engine, particularly during the expansion stroke [15]. This effect has been examined by Yi *et al.* in some unusual engine tests where both NO and HC were dosed in the inlet of a diesel engine, undergoing LTC, and the effect on the NO to NO<sub>2</sub> oxidation observed [16]. However, production diesel engines, which usually operate very lean of stoichiometric, would not usually have unburned hydrocarbons (UHC) present when NO is present – they would have been oxidized by this point in the cycle [8].

Although it has been noted that UHC are not usually present when NO is present during a standard diesel combustion cycle, there are circumstances when this is possible. UHC can be released in the expansion stroke, after most of the combustion has taken place either from crevices, or from the holes of an injector nozzle sack – the latter phenomenon colloquially known as injector dribble [8, 15].

Injector dribble is the expulsion of fuel from a fuel injector after the end of injection (EOI). There is some evidence that links injector dribble to the injector needle closing speed, as well as to off-centre injector needles [17]. Injector dribble does not happen every cycle, but it is known to happen with all the main diesel injector technology types.

A study by Koci *et al.* reported that 75 - 90% of UHC emissions that they observed from a diesel engine were from injector dribble [18]. If injector dribble does occur, the HCs expelled will be located near the injector tip, and this is typically located at the top of the combustion chamber, near the valves, precisely where the high levels of NO<sub>2</sub> have been observed in previous work.

Late cycle UHC emissions can be caused by either injector dribble or the release of UHC from crevices in the expansion stroke. In both cases, the injector and many of the crevices are located near the exhaust valves, which will lead to the UHC emissions being concentrated there, and hence lead to relatively more NO<sub>2</sub> compared to NO near the injector nozzle, the crevices, and hence the exhaust valves. This in turn will lead to proportionally more NO<sub>2</sub> in blowdown part of the exhaust stroke compared to in the displacement part of the exhaust stroke.

This work, therefore, aims to conduct experiments measuring NO, NO<sub>2</sub>, and UHC in the exhaust of the high speed direct injection (HSDI) diesel engine to understand whether UHCs caused by injector dribble or release from crevices are responsible for the previously observed effects on the cyclic NO:NO<sub>2</sub> ratio.

## **METHODOLOGY**

The exhaust from a 500 cc per cylinder diesel research engine was measured using ‘fast’ NO, NO<sub>2</sub>, and UHC analysers. Further details of the engine are shown in Table 1. The engine is not fitted with any exhaust aftertreatment hence the emissions measured are raw engine out emissions. It should be noted that the base engine is the same as that used in a previous work [11], however a number

of changes had been made since this published study, as a result of other projects, including changes to the swirl ratio, the piston material, and the fuel injection system (which was changed from a solenoid operated injector to a piezo injector).

**Table 1: Engine parameters**

Displacement / cylinder	500 cm <sup>3</sup>
Valves per cylinder	2 intake, 2 exhaust
EVO	128 °atdcf
EVC	382 °atdcf
Fuel pressure	2200 bar maximum
Piston bowl	Re-entrant
Injector type	7-hole piezo

Fast NO measurements were made using a Cambustion CLD500 instrument [19, 20]. The NO analyzer uses the chemiluminescence principle coupled with a constant pressure heated sampling system to give a fast sample response time ( $\tau_{10-90\%}$  response time of 2 ms), this time and all other times in this section include both the instrument response time and the sampling time. In addition the sampling system ensures isolation from the temperature and pressure variations seen in engine exhaust [21].

Fast NO<sub>2</sub> measurements were made using a new prototype instrument. Laser-induced fluorescence (LIF) is a long-established analytical technique [22]. The use of LIF for the measurement of NO<sub>2</sub> in atmospheric research is well documented in the literature for both low- [23] and high-pressure regimes [24]. Cambustion extended the applicability of the technique by developing a prototype instrument suitable for the measurement of NO<sub>2</sub> concentration in engine-exhaust gases. The instrument contained a heated-capillary gas-sampling system similar to that used in their other fast gas analyzers and coupled to a miniaturised fibre-coupled LIF detection chamber. Unique features of the instrument were the relative immunity to pressure-fluctuations, high-sensitivity and fast temporal response ( $\tau_{10-90} < 2$  ms). The NO<sub>2</sub> measurement had a  $\tau_{10-90\%}$  response time of 2 ms.

Fast UHC measurements were undertaken with a Cambustion HFR500 instrument [19, 20, 25]. This analyzer uses the flame ionization detection (FID) principle to measure UHCs, and achieves its fast response in a similar in operating premise to the NO and NO<sub>2</sub> analyzers with a heated, constant pressure sampling system. The UHC measurement had a  $\tau_{10-90\%}$  response time of 0.9 ms.

These NO, NO<sub>2</sub>, and UHC sensors were mounted approximately 70 mm downstream of exhaust port at the same point in the manifold, orthogonal one to another. They were logged simultaneously by an AVL IndiSet Advanced 642 at a 0.1 CAD resolution (which corresponds to 9 kHz at an engine speed of 1500 rpm and 15 kHz at 2500 rpm), which also logged cylinder pressure (Kistler 6046ASP-

3-2), inlet (Kistler 4005) and exhaust (Kistler 4011A) manifold pressures, and the injection signal. All of these high-speed parameters were logged for 300 cycles.

Other parameters, including standard emissions measured by a Horiba MEXA-ONE, were logged by Sierra-CP Cadet software at 1 Hz for three minutes. The MEXA-ONE measures CO<sub>2</sub> (both in the inlet and exhaust for EGR rate calculations), CO, THC, NO, NO<sub>2</sub>, NO<sub>x</sub>, and O<sub>2</sub> to a repeatability of 0.5% of full scale for all gases.

Oil and coolant were controlled by a conditioning rig to  $\pm 1$  °C. Inlet air is conditioned using an external rig with a fast-acting dump valve regulating the pressure to an accuracy of  $\pm 0.5\%$  and 10/15 kW heating/cooling controlling the temperature to  $\pm 1$  °C. This air is passed through a 50 L smoothing tank and an 8 L EGR mixing plenum. The engine test cell set-up was otherwise identical to the previous work [11] and additional information about the experimental set-up can be found in [26].

The engine was run on EN590 compliant diesel, which contained no fuel-bound nitrogen or bio components, the detailed fuel composition is shown in Table 2.

**Table 2: Fuel composition**

Cetane Number	53.3
Initial Boiling Point (°C)	172.5
Final Boiling Point (°C)	362.0
Density @ 15°C (kg/L)	0.8312
Aromatics (% m/m)	23.9
Polycyclic Aromatics (% m/m)	2.7
Sulfur (mg/kg)	7.8
FAME (% v/v)	<0.1

Given that our aim was to replicate the unusual results seen in our previous work, as detailed in the introduction, the engine test points were selected to be as close as possible to this previous work [11]. These were selected to give a selection across the speed/load range and are shown in Table 3. Test point 1 is a low speed/load point. Test point 2 is the same speed/load as test point 1 run with cooled, external high pressure EGR; this EGR was inserted into the 8 L mixing plenum upstream of the inlet valves. Test point 4 is a higher speed, mid-load point and test point 3 is between test points 1 and 4.

The original work that we were replicating was intended to understand how the engine out  $\text{NO}_2/\text{NO}_x$  ratio changed in response to engine load transients and as such the engine load was stepped either from the upper to the lower IMEP value shown in Table 3 or vice-versa – one step per test. This was achieved by holding the engine at constant speed at each point with a dynamometer, and changing the engine load (nIMEP) as a step input from a value of 50% of the nominal (75% at test point 4) to the nominal load. The engine stability before the step was ensured by monitoring CoV IMEP and exhaust temperature to ensure they were nominal. In an effort to capture as much of the “after step” effect as possible, the load step was initiated approximately 50 cycles into the data log so that there are around 250 cycles of post-step data.

Fuel injection was closed-loop controlled by a Pi Innovo M670 OpenECU, ensuring a fixed nIMEP, and combustion phasing (CA50). The capabilities of this control are illustrated in Figure 2 which shows the nIMEPs of individual engine cycles at test point 3 as the load is stepped down. It can be seen that immediately the control system reaches within 15% of the target nIMEP, and after 25 cycles, the nIMEP is stable at the new value. This pattern of instantaneous response is typical for all of the points tested.

**Table 3: Test points**

Test point	1	2	3	4
Engine speed (rpm)	1500	1500	2000	2500
nIMEP (upper)* (bar)	7.9	3.8†	6.0	8.5
nIMEP (lower)* (bar)	3.8	n/a	12.2	17.7
Exhaust back pressure (barG)	0.31	0.31	0.8	0.8
Inlet air temperature (°C)	55	55	40	40
Coolant and oil temperature (°C)	90	90	90	90
Target EGR (%)	0	46	0	0
CoV IMEP (upper)* (%)	1.8	3.6	1.4	0.5
CoV IMEP (lower)* (%)	3.3	n/a	3.0	1.6

\*Target nIMEP for the point, the engine load was stepped between the upper and lower values, one step per test.

†No load steps were conducted at this point.

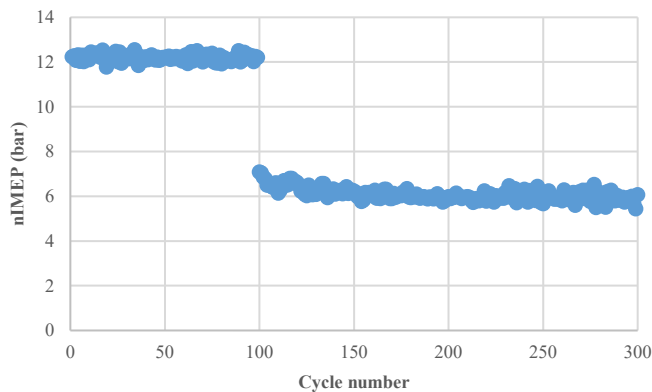


**Figure 2: Cycle-to-cycle IMEP showing a load step down at test point 3**

The fast FID (fFID) used to measure UHCs is known to exhibit a sensitivity to particulate matter emissions. When a particle enters the instrument, its adsorbed hydrocarbons (which will be much higher in concentration compared to the gas the particle is moving in) lead to a “spike” in the signal because of this high concentration [27].

This phenomenon was particularly observed in these tests at test point 2, when there was EGR. As a result, these spikes, which are not representative of the UHC concentrations that are being observed, are filtered out. An example of the unfiltered (blue) and subsequently filtered (black) signals for Test Point 1 are shown in Figure 3.

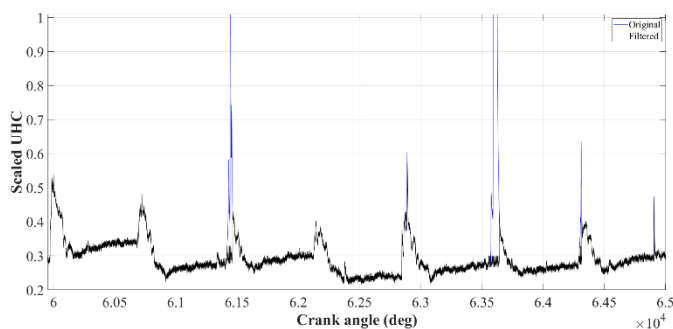


**Figure 3: UHC signal from the fFID showing filtered (black) and unfiltered (blue) signals at test point 1**

The NO<sub>2</sub> (LIF) and NO (chemiluminescence) signals were low-pass filtered, in particular it should be noted that the NO<sub>2</sub> analyser was operating low in its range due to the low overall levels of NO<sub>2</sub> (50-70 ppm) that were observed, so the noise levels were higher than would be desired.



All three of the fast analysers were corrected for any drift observed, as well as for quench in the chemiluminescence and LIF detectors.

The signal from the fast analysers is only representative of the engine cylinder contents when there is gas flow – in other words when the exhaust valves are open. Outside of that time, when the gas is stationary, the reading is simply that of the gas that the probe is exposed to – typically around the value as the exhaust valves closed. As a result to obtain a valid signal, the signal needs only to be taken when the exhaust valves are open. So, once the signals from these analysers had been time-aligned (such that the rise associated with EVO is aligned with EVO), “windowing” was applied, for when the exhaust valves were open, and a mean taken in that window. This is shown in Figure 4.

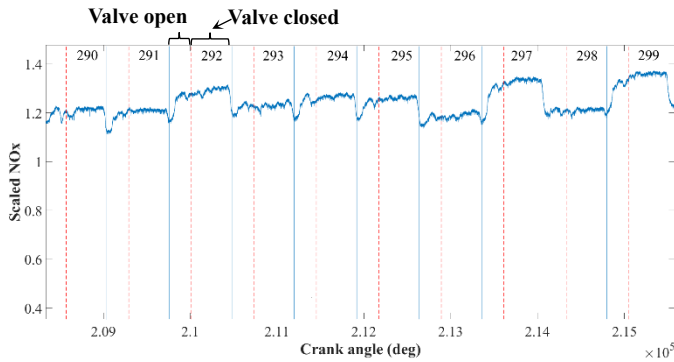


**Figure 4: NO<sub>x</sub> (NO + NO<sub>2</sub>) signal showing EVO and EVC and average window**

For reasons of commercial confidentiality all emissions results presented in this work have been rescaled by dividing by a nominal value (in ppmv) – the same nominal value for all load points and as a result are presented as dimensionless. In addition, where results present NO<sub>x</sub>, it is defined as NO + NO<sub>2</sub>.

## RESULTS

### Cycle resolved NO<sub>x</sub> emissions

The previous work showed a very strong correlation between the  $P_{Max}$  of an individual engine cycle and the NO<sub>x</sub> emitted from that cycle – with a correlation coefficient ( $R^2$ ) greater than 0.95 across all test points [11]. It is of interest to see if this is repeated here, with the engine in a completely different configuration (swirl ratio, piston material, and the fuel injection system are all different). Figure 5

shows the cyclic  $P_{\text{Max}}$  against cyclic  $\text{NO}_x$  at Test Point 1. It can clearly be seen that the strong link observed in the earlier work are repeated here, with a close correlation between cyclic  $P_{\text{Max}}$  and cyclic  $\text{NO}_x$ .

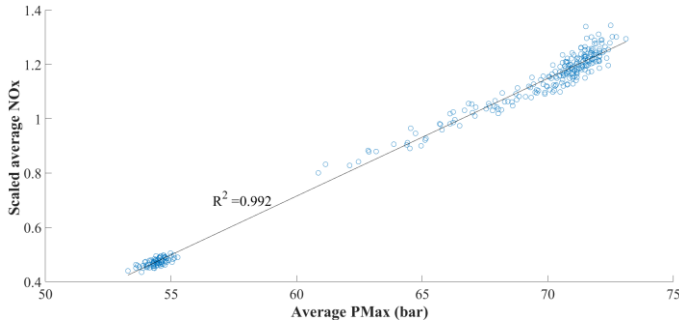


**Figure 5: Cyclic  $P_{\text{max}}$  vs cyclic  $\text{NO}_x$  at test point 1**

Figure 6 presents all of the correlation coefficients of the equivalent plots to Figure 5 for all of the tests undertaken in this work. It shows the correlation coefficient ( $R^2$ ) between  $P_{\text{Max}}$  of an individual engine cycle and the  $\text{NO}_x$  emitted from that cycle across all of the test points. It can be seen that, if anything, the correlations are even stronger than in the previous work, with no test point having an  $R^2 < 0.970$  – there is an extremely strong correlation between the  $P_{\text{Max}}$  of an individual engine cycle and the  $\text{NO}_x$  emitted from that cycle.

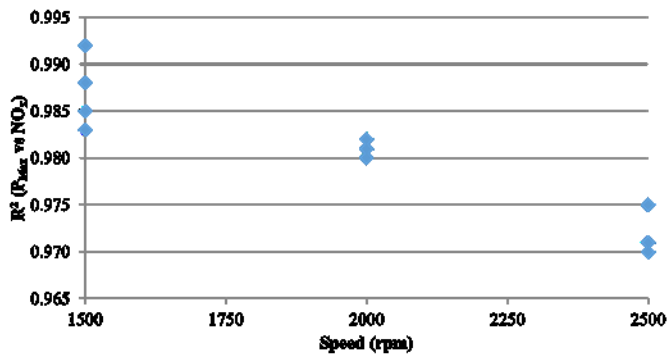


**Figure 6: The correlation coefficients between cyclic  $P_{\text{max}}$  and  $\text{NO}_x$  over all test points**

### Impact of UHC emissions

The main aim of this work was to understand whether UHC emissions near the valves might have an influence on the  $\text{NO}:\text{NO}_2$  ratio. Figure 7 shows the cyclic UHC emissions, plotted against cyclic  $\text{NO}_2$  for 300 cycles at Test Point 1 – each data point represents the emissions from a single engine cycle. The two clusters of data (low UHC, low  $\text{NO}_2$ , and high UHC, high  $\text{NO}_2$ ) represent test points

after (1.9 bar nIMEP) and before (3.8 bar nIMEP) the load step respectively (this particular example shows a step down). There is a good correlation ( $R^2 = 0.806$ ) between the cyclic UHC emission, and the cyclic  $\text{NO}_2$  emission. Much of the scatter on the data could be attributed to the variation in  $P_{\text{Max}}$  from cycle-to-cycle (it may be possible to sensibly deconvolve these two effects, but this has not been attempted in this work). This result is a clear indication that the increase in  $\text{NO}_2$  emissions (and hence the slow NO rise rate previously seen [11]) is consistent with the hypothesis that late cycle UHC emissions near the valves are promoting the conversion of NO into  $\text{NO}_2$ .

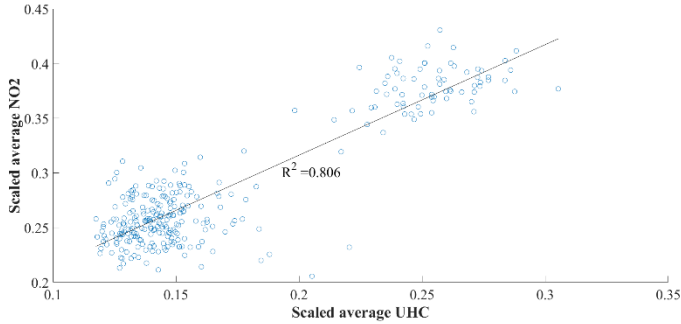


**Figure 7: Rescaled  $\text{NO}_2$  against UHC at test point 1**

Similarly Figure 8 shows the cyclic UHC emissions, plotted against cyclic  $\text{NO}_2$  for 300 cycles at Test Point 4. Again, very similar results are seen here, albeit with a lower correlation (here  $R^2 = 0.57$ ). This lower correlation is to be expected here because at Test Point 4, the load and speed are both higher (2500 rpm, 17.7 bar nIMEP) and so the influence of  $P_{\text{Max}}$  on the cyclic  $\text{NO}_x$  will be higher, hence the scatter on Figure 8 is expected to be higher (again, it may be possible to sensibly deconvolve these two effects, but this has not been attempted in this work).

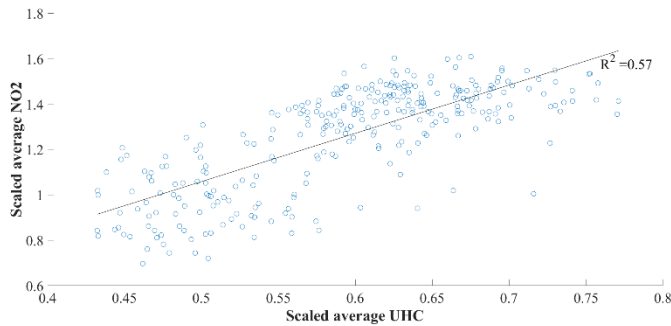


**Figure 8: Rescaled cyclic  $\text{NO}_2$  against cyclic UHC at test point 4**

## Effect of EGR

Test Point 1 was also run with a high level of EGR (Test Point 2), representative of LTC – where the  $\text{NO}_2/\text{NO}_x$  ratio is very high, but overall  $\text{NO}_x$  levels are low (see [10] for details). Figure 9 shows the  $\text{NO}_2/\text{NO}_x$  ratio against cyclic UHC with EGR. Because of limitations in running the engine, it was not possible to run the engine with exactly the same levels of EGR each time, so minor variations are apparent (the EGR rate varies between 45.18% and 46.71%). Again, each point represents the one of each of 300 cycles, and here no load step was undertaken. It can clearly be seen from Figure 9 that, when differences in EGR are taken into account, the correlation between UHC and cyclic  $\text{NO}_2$  (or in this case cyclic  $\text{NO}_2/\text{NO}_x$  ratio) is still visible – although the addition of EGR has masked the effect to some extent (here  $0.31 < R^2 < 0.36$ ). This reduction in correlation with EGR can be attributed to the overall very low levels of  $\text{NO}_x$  emissions observed at this test point with high levels of EGR, which mean that the signal to noise ratio of the instrumentation is poorer than at other operating conditions. In addition, the overall levels of  $\text{NO}_2$  are already very high (65% - 80%) meaning that, inevitably, there is less  $\text{NO}$  to convert to  $\text{NO}_2$  by this mechanism.

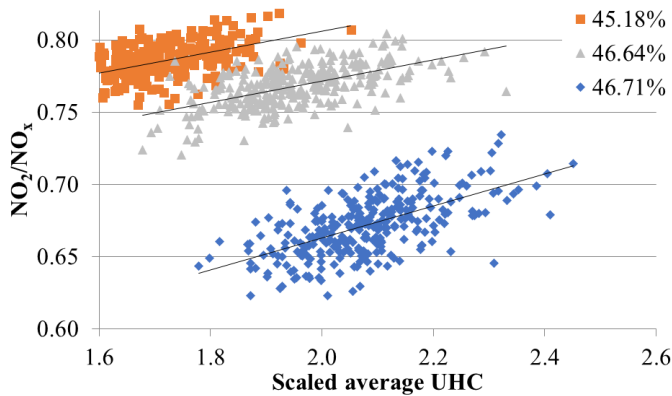


**Figure 9:  $\text{NO}_2/\text{NO}_x$  ratio against cyclic UHC at test point 2**

## Results over all test points

It is possible to combine data from repeats, and ultimately from all of the tests conducted. Figure 10 shows the cyclic UHC emissions, plotted against cyclic  $\text{NO}_2$  for all of the individual cycles logged at Test Point 4 (three repeats were undertaken - 900 cycles total). The repeatability between the three runs is clearly seen, as is the link between the cyclic UHC emissions and cyclic  $\text{NO}_2$  emissions.

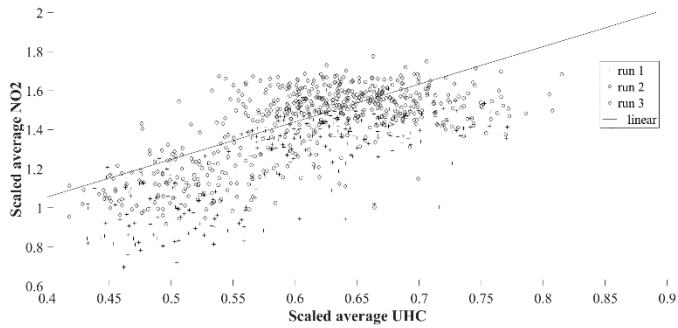


**Figure 10: Individual cycle NO<sub>2</sub> against cyclic UHC for all logged cycles at test point 4**

Figure 11 shows the mean cyclic NO<sub>2</sub> against the cyclic UHC for all of the test points (both before and after the load steps where applicable). Each point on this graph represents the mean of the number of cycles before or after the load step – this number will vary slightly depending on exactly when the load step was initiated relative to data logging starting, however, there will be approximately 20% of cycles logged before the load step, and 80% of cycles logged after the load step (see the methodology section). The link between cyclic NO<sub>2</sub> and cyclic UHC is clear on this plot. The correlation coefficient is higher ( $R^2 = 0.99$  compared to  $R^2 = 0.89$ ) for the cycle average after the load step than the cycle average before the load step due to the fact that the sample sizes are not equal – substantially more data being taken after the load step.

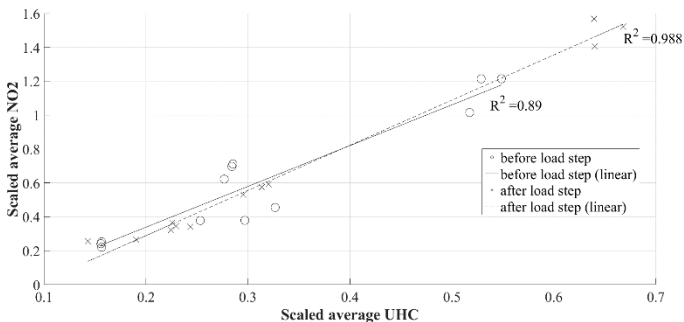


**Figure 11: Mean cyclic NO<sub>2</sub> against cyclic UHC for all logged test points**

### Performance of new NO<sub>2</sub> instrument

In this work, NO<sub>2</sub> was measured by a new fast analyser which measured NO<sub>2</sub> directly with crank angle resolution using LIF, rather than the previous methods of passing the sample through a NO<sub>x</sub> converter, for the first time. It is of interest to evaluate the performance of this instrument. Figure 12 shows the comparison between the fast and the slow (MEXA-ONE) analysers for both this data (the orange squares) taken with the new LIF instrument, and a previous data set (the blue diamonds) at the same engine operating points (but taken

with a different engine configuration – see the methodology section) taken by the previous method of passing the exhaust sample through a NO<sub>x</sub> converter.

Looking at Figure 12 it can be seen that both data sets (instruments) are close to the unity slope line, but perhaps the data taken from the older CLD instrument is closer to the line, however the magnitudes of NO<sub>2</sub> between the two data sets are different, and it is not known how the CLD instrument would have behaved at higher NO<sub>2</sub> levels. The big change moving from the CLD to the LIF is the magnitude of the error bars (which correspond to  $\pm\sigma$ ). The average standard deviation ( $\sigma$ ) of the measurement has decreased by nearly an order of magnitude from 0.025 rescaled NO<sub>2</sub> with the CLD instrument, to 0.003 rescaled NO<sub>2</sub> with the LIF instrument (despite the higher NO<sub>2</sub> values measured by the LIF instrument). This reduction in  $\sigma$  gives a substantial increase in confidence in the results from the new instrument, and demonstrates it to be a valuable tool in fast NO<sub>2</sub> measurement compared with the previous state-of-the-art.

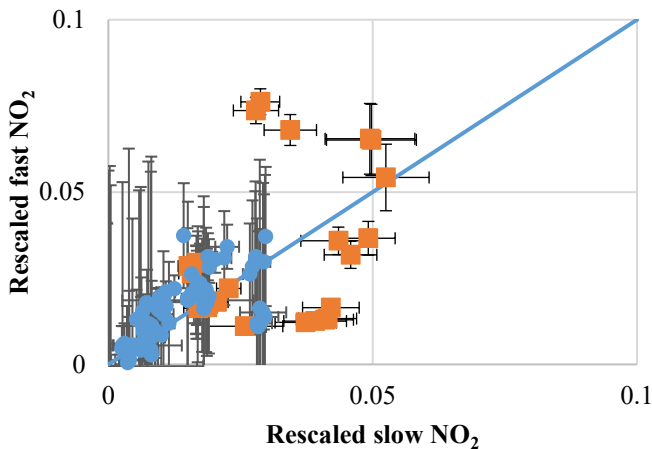


**Figure 12: Comparison of NO<sub>2</sub> measurements from two fast and the slow analyser**

## CONCLUSIONS

Crank-angle resolved NO, NO<sub>2</sub>, and UHC measurements have been taken from a high-speed light duty diesel engine at a variety of engine test conditions from low load and speed to high load and speed with and without EGR.

A previously seen link between the  $P_{Max}$  of an individual engine cycle and the NO<sub>x</sub> emissions from that cycle have been repeated here, with a completely different engine configuration. Similarly, a previously seen slow NO rise rate, which is associated with an in cylinder stratification of NO and NO<sub>2</sub> as the exhaust valves open, has again been repeated with this different engine configuration (notably, compared to the previous work, the engine has a different swirl ratio, piston material, and fuel injection system).

It has been demonstrated that there is a strong correlation between the UHC emissions from an individual engine cycle and the NO<sub>2</sub> emissions from that cycle. Higher cycle UHC emissions can be caused by either injector dribble or release from the crevices, both of which are common in all diesel engines. Both of these reasons will cause the UHC to be located near the valves. Here it is promoting NO to NO<sub>2</sub> conversion, hence increasing (proportionally) the amount of NO<sub>2</sub> near the exhaust valves. This is the reason for the slow NO rise rate during blowdown, which is associated with in-cylinder stratification of NO and NO<sub>2</sub>.

This correlation attributable to this mechanism is reduced by cyclic variation in overall NO<sub>x</sub> emissions, which can be attributed to cyclic variations in P<sub>Max</sub>. In addition the correlation is weaker at high levels of EGR, where overall NO<sub>x</sub> emissions are low, and NO<sub>2</sub> levels, as a proportion of total NO<sub>x</sub>, are much higher (which would weaken the contribution of conversion by this mechanism).

A new instrument to measure NO<sub>2</sub> directly with crank angle resolution using a LIF technique has been tested for the first time and the results presented. This LIF instrument provides a much less noisy measurement of crank angle resolved NO<sub>2</sub> compared to the CLD instruments that are currently used for this purpose. In addition, that this in cylinder stratification of NO and NO<sub>2</sub> has now been observed using two different types instrumentation substantially decreases the possibility that any results are due to instrumentation effects.

Overall, in this work, the phenomenon of in-cylinder stratification in NO and NO<sub>2</sub> has been observed at all operating conditions, and a strong correlation with cycle UHC emissions provides confidence that this may be the cause.

## NOMENCLATURE

CA50	Angle of 50% mass fraction burned
CAD	Crank Angle Degree
CFD	Computational Fluid Dynamics
CLD	ChemiLuminescence Detector
DOC	Diesel Oxidation Catalyst
EGR	Exhaust Gas Recirculation
EOI	End Of Injection
EVC	Exhaust Valve Closing
EVO	Exhaust Valve Opening
ffID	fast Flame Ionisation Detection
FID	Flame Ionisation Detection
HC	HydroCarbon
HSDI	High Speed Direct Injection

IMEP	Indicated Mean Effective Pressure
LIF	Laser Induced Fluorescence
LNT	Lean NO <sub>x</sub> Trap
LTC	Low Temperature Combustion
nIMEP	net Indicated Mean Effective Pressure
NO <sub>x</sub>	Oxides of Nitrogen
P <sub>Max</sub>	Maximum Cylinder Pressure
ppmv	Parts per million (by volume)
RDE	Real Driving Emissions
SCR	Selective Catalytic Reduction
SOI	Start of Injection
UHC	Unburned HydroCarbon
$\sigma$	Standard deviation

## ACKNOWLEDGMENTS

The authors would like to thank Jaguar Land Rover and the University of Oxford John Fell Fund for financial support. The authors would like to thank Nick Papaioannou and the Department of Engineering Science technicians and maintenance teams for undertaking much of the engine testing and facilities support.

## REFERENCES

1. Senecal, P.K. and F. Leach, *Diversity in transportation: Why a mix of propulsion technologies is the way forward for the future fleet*. Results in Engineering, 2019. **4**, 100060, doi:10.1016/j.rineng.2019.100060
2. Leach, F., et al., *Comparing the Effect of Fuel/Air Interactions in a Modern High-Speed Light-Duty Diesel Engine*. SAE Technical Paper 2017-24-0075, doi:10.4271/2017-24-0075
3. Ladommatos, N., et al., *Effects of EGR on Heat Release in Diesel Combustion*. SAE Technical Paper 980184, 1998, doi:10.4271/980184



4. Johnson, T.V., *Diesel Emissions in Review*. SAE International Journal of Engines, 2011. **4**(1): p. 143-157, doi:10.4271/2011-01-0304
5. Johnson, T.V., *Review of Vehicular Emissions Trends*. SAE International Journal of Engines, 2015. **8**(3): p. 1152-1167, doi:10.4271/2015-01-0993
6. Stadlbauer, S., et al., *DOC Temperature Control for Low Temperature Operating Ranges with Post and Main Injection Actuation*. SAE Technical Paper 2013-01-1580, doi:10.4271/2013-01-1580
7. Harris, T.M., et al., *Modeling of Close-Coupled SCR Concepts to Meet Future Cold Start Requirements for Heavy-Duty Engines*. SAE Technical Paper 2019-01-0984, doi:10.4271/2019-01-0984
8. Heywood, J.B., *Internal combustion engine fundamentals*. Vol. 930. 1988: Mcgraw-hill New York.
9. Rößler, M., et al., *Formation of Engine Internal NO<sub>2</sub>: Measures to Control the NO<sub>2</sub>/NO<sub>x</sub> Ratio for Enhanced Exhaust After Treatment*. SAE International Journal of Engines, 2017. **10**(4): p. 1880-1893, doi:10.4271/2017-01-1017
10. Leach, F., M. Davy, and M. Peckham, *Cyclic NO<sub>2</sub>:NO<sub>x</sub> ratio from a diesel engine undergoing transient load steps*. International Journal of Engine Research, doi:10.1177/1468087419833202
11. Leach, F., M. Davy, and M. Peckham, *Cycle-to-Cycle NO and NO<sub>x</sub> Emissions From a HSDI Diesel Engine*. Journal of Engineering for Gas Turbines and Power, 2019. **141**(8), doi:10.1115/1.4043218
12. Nelson, P.F. and B.S. Haynes, *Hydrocarbon-NO<sub>x</sub> interactions at low temperatures—I. Conversion of NO to NO<sub>2</sub> promoted by propane and the formation of HNCO*. Symposium (International) on Combustion, 1994. **25**(1): p. 1003-1010, doi:10.1016/S0082-0784(06)80737-X
13. Hori, M., et al., *An experimental and kinetic calculation of the promotion effect of hydrocarbons on the NO-NO<sub>2</sub> conversion in a flow reactor*. Symposium (International) on Combustion, 1998. **27**(1): p. 389-396, doi:10.1016/S0082-0784(98)80427-X
14. Hori, M., et al., *Temperature dependence of NO to NO<sub>2</sub> conversion by n-butane and n-pentane oxidation*. Proceedings of the Combustion Institute, 2002. **29**(2): p. 2219-2226, doi:10.1016/S1540-7489(02)80270-X
15. Stone, R., *Introduction to internal combustion engines*. 2012: Palgrave Macmillan.
16. Yu, X., S. Yu, and M. Zheng, *Hydrocarbon impact on NO to NO<sub>2</sub> conversion in a compression ignition engine under low-temperature combustion*. International Journal of Engine Research, 2019. **20**(2): p. 216-225, doi:10.1177/1468087417745441
17. Moon, S., et al., *End-of-injection fuel dribble of multi-hole diesel injector: Comprehensive investigation of phenomenon and discussion on control strategy*. Applied Energy, 2016. **179**: p. 7-16, doi:10.1016/j.apenergy.2016.06.116

18. Koci, C.P., et al., *The effects of fuel–air mixing and injector dribble on diesel unburned hydrocarbon emissions*. International Journal of Engine Research, 2019. **20**(1): p. 105-127, doi:10.1177/1468087418821827
19. Schurov, S., et al., *Fast Response NO/HC Measurements in the Cylinder and Exhaust Port of a DI Diesel Engine*. SAE Technical Paper 980788, 1998, doi:10.4271/980788
20. Reavell, K.S.J., et al., *Simultaneous Fast Response NO and HC Measurements from a Spark Ignition Engine*. SAE Technical Paper 971610, 1997, doi:10.4271/971610
21. Leach, F.C.P., et al., *An optical method for measuring exhaust gas pressure from an internal combustion engine at high speed*. Review of Scientific Instruments, 2017. **88**(12): 125004, doi:10.1063/1.5005161
22. Tango, W.J., J.K. Link, and R.N. Zare, *Spectroscopy of K<sub>2</sub> Using Laser-Induced Fluorescence*. The Journal of Chemical Physics, 1968. **49**(10): p. 4264-4268. doi:10.1063/1.1669869
23. Matsumoto, J. and Y. Kajii, *Improved analyzer for nitrogen dioxide by laser-induced fluorescence technique*. Atmospheric Environment, 2003. **37**(34): p. 4847-4851, doi:10.1016/j.atmosenv.2003.08.023
24. Parra, J. and L.A. George, *Development of an ambient pressure laser-induced fluorescence instrument for nitrogen dioxide*. Applied Optics, 2009. **48**(18): p. 3355-3361, doi:10.1364/AO.48.003355
25. Cheng, W.K., T. Summers, and N. Collings, *The fast-response flame ionization detector*. Progress in Energy and Combustion Science, 1998. **24**(2): p. 89-124, doi:10.1016/S0360-1285(97)00025-7
26. Leach, F., et al., *Comparing the effect of a swirl flap and asymmetric inlet valve opening on a light duty diesel engine*. SAE Technical Paper 2017-01-2429, doi:10.4271/2017-01-2429
27. Sun, J.H. and S.H. Chan, *A time-resolved measurement technique for particulate number density in diesel exhaust using a fast-response flame ionization detector*. Measurement Science and Technology, 1997. **8**(3): p. 279-286, doi:10.1088/0957-0233/8/3/010